PCCP

Accepted Manuscript

ROYAL SOCIETY OF CHEMISTRY

www.rsc.org/pccp

Received 00th January 20xx,
Accepted 00th January 20xx

DOI: 10.1039/x0xx00000x

www.rsc.org/

Dye adsorption mechanisms in TiO2 films, and its effects on photodynamic and photovoltaic properties in dye-sensitized solar cell

Kyung-Jun Hwang,[a] Wang-Guen Shim,[*,b] Youngjin Kim,[c] Gunwoo Kim,[c] Chulmin Choi,[a] Sang Ook Kang[d] and Dae Won Cho[*,d,e]

The adsorption mechanism for N719 dye on a TiO_2 electrode was examined by the kinetic and diffusion models (*pseudo*-first order, *pseudo*-second order, and intra-particle diffusion models). Among these methods, the observed adsorption kinetics are well-described using the *pseudo*-second order model. Moreover, the film diffusion process was the main controlling step of adsorption, which was analysed using a diffusion-based model. The photodynamic properties in dye-sensitized solar cells (DSSC) were investigated using time-resolved transient absorption techniques. The photodynamics of the oxidized N719 species were shown to be dependent on the adsorption time, and also the adsorbed concentration of N719. The photovoltaic parameters (J_{sc}, V_{oc}, *FF* and η) of this DSSC were determined in terms of the dye adsorption amounts. The solar cell performance correlates significantly with charge recombination and dye regeneration dynamics, which are also affected by the dye adsorption amounts. Therefore, the photovoltaic performance of this DSSC can be interpreted in terms of the adsorption kinetics and the photodynamics of oxidized N719.

Introduction

Dye-sensitized solar cells (DSSC) have attracted considerable attention as promising candidates for the production of low cost solar energy. Since they were first reported in 1991,[1] DSSCs have been the subject of extensive fundamental and experimental research, with reported photovoltaic conversion efficiencies exceeding 12% when using porphyrin dyes.[2] Recently, efficiencies exceeding 20% have been demonstrated using perovskite materials as photosensitizers.[3]

As shown in Scheme 1, a typical DSSC consists of a transparent conducting oxide (TCO) glass electrode coated with mesoporous and nanocrystalline TiO_2, dye molecules adsorbed onto the TiO_2 surface, a redox couple electrolyte such as triiodide/iodide (I_3^-/I^-), and a counter electrode such as platinum or carbon.[4] Photoelectric current is initiated by electron injection from the excited dye to the TiO_2 electrode upon irradiation. Concurrently, dye oxidation produces cation radicals ($dye^{+\bullet}$, i.e. holes). The injected electron should travel to the TCO electrode through TiO_2. However, some injected electrons on the TiO_2 surface recombine with the oxidized $dye^{+\bullet}$, a process known as charge recombination (CR).[5] On the other hand, the oxidized dye is subsequently reduced by the electrolyte containing I^-, which in turn is regenerated by the reduction of I_3^- at the counter electrode. This constitutes the dye-regeneration (DR) process.[5] In general, rapid DR and slow CR processes are desirable for obtaining high solar conversion efficiency.

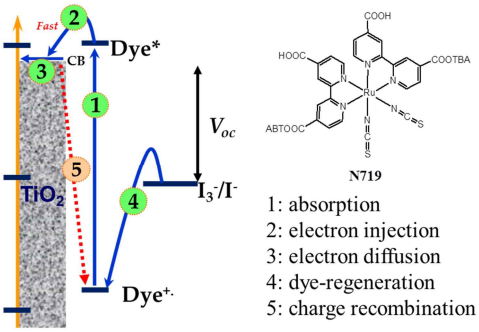

Scheme 1. Energy-level diagram of DSSC.

We have reported that charged species, such as photoelectrons and oxidized dyes, are distributed in the front of a TiO_2 film. The photodynamics are affected by the thickness of the TiO_2 film and the presence of a scattering layer.[6] Therefore, the penetration depth of light is a very important factor for both CR and DR dynamics. The photodynamic properties for the CR and DR processes depend on the distribution of electrons and the radical $dye^{+\bullet}$ (holes), which can be influenced by the concentration of adsorbed dye. These are particularly critical factors to the photocurrent and increasing photon absorption.

In this work, we have investigated the correlations between the photovoltaic performance and the adsorption mechanism. The photodynamic properties for CR and DR processes have also been studied using time-resolved transient absorption spectroscopic measurements. Based on experimental results, we report that the adsorption behaviours of N719 on TiO_2 influence photodynamic properties and therefore affect the DSSC performance.

[a] *Mechanical and Aerospace Engineering, University of California at San Diego, La Jolla CA 92093, USA. E-mail: kyhwang@ucsd.edu; cnchoi@ucsd.edu*
[b] *Center for Technology in Water and Wastewater, School of Civil and Environmental Engineering, University of Technology Sydney, Broadway, NSW 2007, Australia. E-mail: wgshim527@hanmail.net*
[c] *Material Science and Engineering, University of California at San Diego, La Jolla CA 92093, USA. E-mail: yjk019@ucsd.edu; gunwoo@eng.ucsd.edu*
[d] *Department of Advanced Materials Chemistry, Korea University (Sejong Campus), Sejong 339-700, Korea. E-mail: sangok@korea.ac.kr; dwcho@ korea.ac.kr*
[e] *Center for Photovoltaic Materials, Korea University (Sejong Campus), Sejong 339-700, Korea.*

Experimental

Preparation of TiO_2 electrode

A 3 cm × 3 cm fluorine-doped tin dioxide conducting glass (FTO; Pilkington, TEC-8) was cleaned with acetone in an ultrasonic bath for 15 min, rinsed with ethanol and water, and dried in an oven at 80 °C for 1 h. The dry weight of each FTO glass was measured using a digital balance. A mask, with an open area of 2 cm × 2 cm, was placed onto the FTO glass to allow for deposition of the TiO_2 electrode. TiO_2 paste with uniform particle size (20 nm) was synthesized according to the literature,[7] and was placed in the mask opening using a screen printing technique (SM-S320, Sun Mechanix). The screen-printed TiO_2 paste/FTO substrates were kept in a clean box and were saturated with ethanol for approximately 10 min in order to reduce the surface irregularity of the coated paste. Then the TiO_2 film was sintered at 500 °C for 30 min. An approximately 12 µm-thickness TiO_2 film was deposited onto the FTO glass substrate. The weight of TiO_2 electrode deposited on the FTO glass can be determined by the subtraction from the total weight of the dried TiO_2 film and FTO glass to the uncoated FTO glass.

Fabrication of DSSC

The fabrication method is described in elsewhere.[8] Two pinholes for injecting the electrolyte were drilled on the rinsed FTO glass using a drilling machine (DREMEL KIT 335, BOSCH). The Pt-counter electrode, prepared on FTO glass using 0.05 M H_2PtCl_6 (Aldrich) solution, was annealed at 400 °C for 30 min in air. The prepared photoelectrode and counter electrode were sealed with a hot-melt sealing sheet (SX 1170-60, Solaronix). The preparation of the DSSC was completed by injecting a redox electrolyte consisting of 0.6 M PM II (1-methyl-3-propylimidazolium iodide), 0.03 M I_2, 0.1 M guanidinium thiocyanate and 0.5 M 4-tertbutylpyridine into a mixture of acetonitrile and valeronitrile (v/v = 85:15).

Characterization of photoelectric and photodynamic properties of DSSC

The current-voltage (*J-V*) measurement was performed for the active cell area of 0.36 cm^2 using a Keithley 4300 source meter under 100 mW/cm^2 irradiation (Oriel, 94041A 450 W). The light intensity was calibrated using a Si reference diode equipped with an air mass 1.5-G filter (KG5). The *J-V* curves were used to calculate the short-circuit current (J_{sc}), open-circuit voltage (V_{oc}), fill factor (*FF*), and solar conversion efficiency (η) of the DSSC. The incident photon-to-current efficiency (IPCE) was measured as a function of wavelength from 300 to 900 nm using the IPCE measurement apparatus (QEX7, PV Measurements).

Nanosecond transient absorption measurements were carried out using laser flash photolysis;[6,9] the DSSC was excited by nanosecond laser pulses (540 nm, 10 Hz repetition rate) produced by an optical parametric oscillator (Continuum, Surelite OPO) pumped by the third harmonic generation (355 nm, FWHM = 4.5 ns) from a Q-switched Nd:YAG laser (Continuum, Surelite II-10). Excitation pulses were attenuated by neutral density (ND) filters to adjust the pulse intensity incident on the sample to < 30 µJ/cm^2, which can be further changed by the ND filters. Transient adsorption measurement was made using probe light from a xenon arc lamp (ILC Technology, PS 300-1), which was passed through a band-pass filter with FWHM of ~20 nm to measure the temporal profiles, and then focused onto the sample. Temporal profiles were measured with a monochromator (DongWoo Optron, Monora 500i) equipped with a fast photomultiplier tube (Zolix Instruments, CR 131) and a digital oscilloscope (Tektronix, TDS-784D). The reported signals were averaged over the course of 3,000 events in order to obtain satisfactory signal to noise ratios. The transient absorption spectra were measured by an intensified charge-coupled device (ICCD, Ando, iStar).

Adsorption analysis

The adsorption kinetics was measured using the apparatus as described elsewhere.[10] The N719 dye was purchased from Solaronix (0.5 mM N719 in ethanolic solution). The TiO_2 films were dipped into a 25 mL adsorption vessel containing 10 mL of 0.5 mM N719 solution and a stirrer rotated at 100 rpm. Samples were withdrawn regularly from the adsorption vessel via micropipette for analysis. During the adsorption process, the N719 residuals were determined by monitoring the absorbance changes at 510 nm using a UV spectrophotometer (UV-160A, Shimadzu). Contrast to conventional method, this method can be used to directly investigate adsorption kinetics without consideration of desorption procedures. The amount of N719 at equilibrium on the TiO_2 films was calculated using equation (1):

$$q = \frac{(C_o - C)}{w} V \qquad (1)$$

where *q* (mmol/g) is the equilibrium amount of N719 adsorbed on the TiO_2 film, C_0 and *C* (mmol/l) are the dye concentrations at initial and equilibrium states, respectively. The volume *V* (litre) is the volume of the solution, and *w* (g) is the mass of the TiO_2 film.

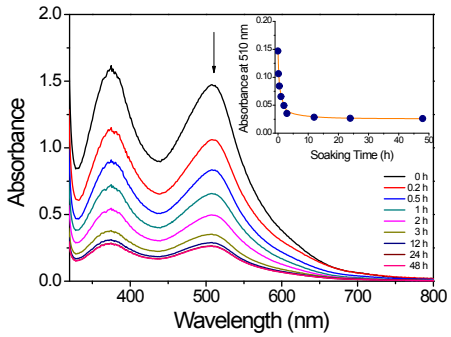

Fig. 1 The absorption spectra for N719 residue (initial concentration: 0.5 mM in ethanol) measured at various dye adsorption times using a cell with 2 mm path length.

Results and Discussion

Dye adsorption kinetics

Fig. 1 shows the absorption spectra of N719 residuals after the dye-impregnation into the TiO_2 film. The spectra were measured at different soaking (adsorption) times in ethanol solution. The spectra exhibit typical absorption bands of N719 at around 375 and 510 nm. These bands decreased drastically early in the adsorption process, then changed less dramatically at later times as shown in inset of Fig. 1.

The adsorption rate constant is one of the key parameters for understanding the adsorption mechanism and the practical adsorption-related process.[11,12] The adsorption concentrations of N719 were determined using the absorption spectra shown in Fig. 1. As shown in Fig. 2a, the adsorption amount of N719 increased markedly within the first 3 h. This fast adsorption is attributed to the excellent adsorbing ability of the carboxylate groups of N719. The carboxylates can be adsorbed either at the defect sites or at the hydroxyl groups on the surface of the porous TiO_2 electrode. The adsorption amount of N719 increases smoothly, but at a lesser rate, from approximately 3 to 12 hours. At 12 h, the TiO_2 surface is saturated and the adsorption process tapers off. This adsorption trend is typical for organic materials on porous metal oxides.[13,14]

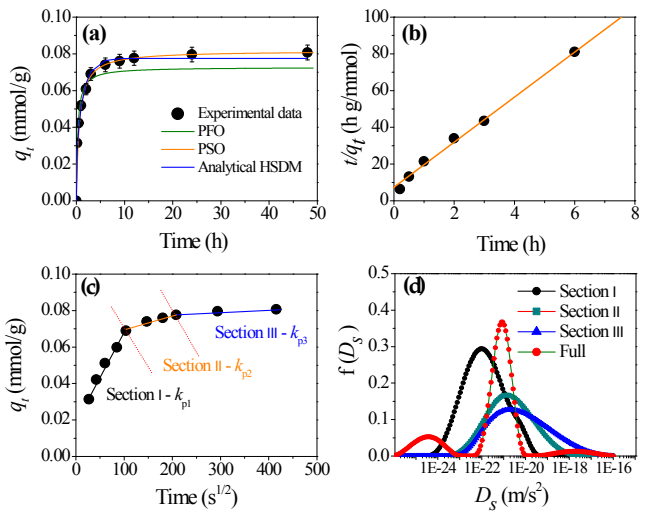

Fig. 2. (a) Experimental kinetic data for N719 adsorption on TiO_2 films and fitted kinetic profiles using various models; (b) experimental and fitted kinetic profiles using the pseudo-second order (PSO) kinetic model for N719 adsorption on TiO_2 films; (c) experimental and fitted kinetic profiles using the intra-particle diffusion (Weber-Morris) model for N719 adsorption on TiO_2 films; (d) the distribution functions of the N719 diffusion coefficient.

The qualitative tendency for N719 adsorption on TiO_2 films was analysed using two well-known representations of adsorption kinetics: a pseudo-first order (PFO) model, and a pseudo-second order (PSO) model. The adsorption parameters listed in Table 1 can be determined using the fitted profiles from the PFO and PSO models, as shown in Fig. 2a.

The PFO equation (eq. 2)[15,16] proposed by Lagergren is:

$$\log(q_e - q_t) = \log q_e \frac{k_1}{2.303} t \qquad (2)$$

where q_e and q_t are the adsorption amounts (mmol/g) of N719 onto TiO_2 at equilibrium and at time t (h), respectively. This equation has been used to describe adsorption phenomena under specific conditions, such as low concentration of solute or in a state of equilibrium. The rate constant for adsorption is k_1 (h^{-1}). The q_e value fitted by the PFO model is significantly smaller than the experimental q_e value (Table 1), which suggests the PFO model may not be applicable for this N719/TiO_2 system.

In order to compensate for the deviation from the PFO model, the PSO equation has been applied as expressed in equation (3):[15,17]

$$\frac{t}{q_t} = \frac{1}{k_2 q_e^2} + \frac{1}{q_e} t \qquad (3)$$

where k_2 (h·g/mmol) is the rate constant for second-order adsorption. The PSO model is appropriate for explaining the chemisorption kinetics of highly heterogeneous adsorbents, and the PSO rate equation is in agreement with experimental results for the kinetics of N719 adsorption onto porous TiO_2 with a correlation coefficient (R^2) of 0.999. Thus, it is reasonable to conclude that chemisorption is the main rate-controlling step for the N719 adsorption onto the surface of TiO_2 electrode.

The experimental data and fitted PSO kinetic profiles derived from the kinetic model for N719 adsorption on TiO_2 films are shown in Fig. 2b. The concentration in the PSO model does not converge to zero at t=0 because TiO_2 electrodes typically have heterogeneous sites and defects at the surface.[18] Adsorption sites such as –OH, -OH_2, and -O- make analysis of adsorption kinetics for TiO_2 surfaces more difficult. Single bridging vacancies, double bridging vacancies, and lattice vacancies are other imperfections that can exist at the electrode surface.[19]

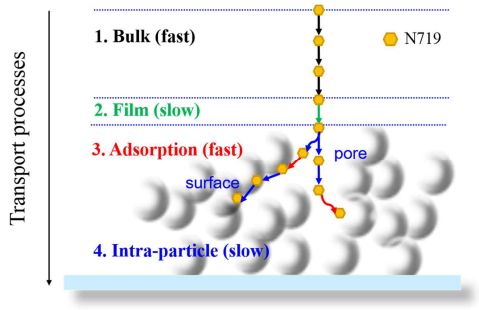

Scheme 2. Transport processes in adsorption by TiO_2 adsorbent.

The diffusion-based kinetic model has also been used to explain the influence of diffusion on the adsorption process in heterogeneous systems. As shown in scheme 2, the transport resistances in the adsorption process can be classified into four types: 1) bulk, 2) film, 3) adsorption, and 4) intra-particle diffusion processes. The intra-particle diffusion model consists of a pore (or crack) diffusion and a surface diffusion. Usually, the bulk and the adsorption processes are much faster than the other two processes. Thus, these two processes are not investigated as thoroughly in the analysis of heterogeneous adsorption systems. On the other hand, mass transfer is a very important and highly varied process. This process depends on

the combined nature of the adsorbent and the adsorbate, as well as the overall conditions of the adsorption process. Therefore, it is more likely that either the film or intra-particle (especially pore) diffusion resistance controls the adsorption process and becomes the limiting step.[20]

Among many adsorption diffusion models, the Weber-Morris model and homogeneous solid diffusion model have been widely used to determine the rate-controlling step of adsorption. The intra-particle diffusion kinetic model based on the Weber-Morris equation (eq. 4):

$$q_t = k_{\mathrm{pi}} t^{1/2} + C \qquad (4)$$

is used to fit the adsorption data and to investigate the adsorption mechanism,[15,21] where k_{pi} is the intra-particle diffusion rate constant for adsorption at stage *i* (g/mmol·h$^{1/2}$), and *C* is the intercept that represents the boundary layer thickness (mg/g). According to equation (4), the plot of *q* versus $t^{1/2}$ should be a straight line with slope k_{pi} and y-intercept *C*. When this linear plot passes through the origin (i.e. *C*=0), then the intra-particle diffusion is considered to be the rate-controlling step, and the film diffusion is negligible. However, when the straight line does not pass through the origin (i.e. *C* has a value), this indicates that there is a difference the rates of mass transfer in the initial and final steps of adsorption, and that the film diffusion is involved simultaneously along with intra-particle diffusion. Both are can be considered as the rate-controlling step.

The linearized plots of the adsorption amount of N719 versus the square root of time (*q* vs. $t^{1/2}$) were obtained, and the results are shown in Fig. 2c. The plots are tri-phasic in nature. Three different slopes are required to fit the data properly, indicating that three types of diffusion influence the rate-limiting steps. Because the straight lines do not pass through zero, the lines for film and intra-particle diffusions are combined.

The intra-particle diffusion rate constants for the stepwise adsorption decrease in the following order: $k_{\mathrm{p1}} > k_{\mathrm{p2}} > k_{\mathrm{p3}}$ (Table 1). The steep slope shown for k_{p1} represents the fast adsorption process of N719 dye, in that the dye molecules are transferred onto the electrodes by film diffusion.[22] The second slope k_{p2} is more gradual and reflects the process whereby the N719 molecules are slowly diffusing and adsorbing into the pores. The flat slope k_{p3} is attributed to the adsorption process at equilibrium, where the adsorbate diffuses very slowly into the micropores because the concentration in the solution has decreased.[23] The intra-particle diffusion rate constants for the stepwise adsorption are listed in Table 1. Based on the Weber-Morris approach, it can be concluded that both film and intra-particle diffusion processes are involved in controlling the rate of adsorption.

In order to investigate the contribution of film diffusion in the system further, a homogeneous solid diffusion model (HSDM) has been applied according to equation (5):[24,25]

$$\frac{\bar{q}}{q_\infty} = 1 - \frac{6}{\pi^2}\sum_{n=1}^{\infty}\frac{1}{n^2}\exp\left(-\frac{D_i n^2 \pi^2 t}{R^2}\right) \qquad (5)$$

where $\bar{q}$ is the average concentration at any particular time (mmol/g), q_∞ is the solute concentration in the solid corresponding to an infinite time (mmol/g), *n* is number of terms, *t* is the time, D_{i} is the effective intra-particle diffusion coefficient (m^2/min), and R is the TiO_2 particle radius. The detailed explanation is given elsewhere.[11,12,26]

Integrating this equation over the range of diffusion coefficients gives the diffusion coefficient distribution function (DCDF), which is helpful to characterize the adsorption kinetics.[27,28] The distribution function that is based on the integral equation can be written as follows:

$$\frac{\bar{q}}{q_\infty} = \int_{D_{\min}}^{D_{\max}} 1 - \frac{6}{\pi^2}\sum_{n=1}^{\infty}\frac{1}{n^2}\exp\left(-\frac{D_i n^2 \pi^2 t}{R^2}\right) f(D_s)\,dD \qquad (6)$$

where *R* is the particle radius, D_{s} is the diffusivity, $D_{\min}$ is the minimum of the diffusion coefficient, $D_{\max}$ is the maximum of the diffusion coefficient, and $f(D)$ is the distribution function of the diffusivity. Additionally, the Nelder-Mead (or downhill simplex) method[29] and the generalized nonlinear regularization method were used to determine *D* as well as the distribution function for D. In order to determine the controlling step of the system, three different entities (section I – k_{p1}, section II – k_{p2}, section III – k_{p3} and whole) are used to describe the experimental results given in the Weber-Morris plot presented in Fig 2(c). As a result, Fig. 2(d) compares the distributions of the calculated diffusion coefficients for N719 adsorbed on the surface of the TiO_2 electrode. The distribution curves for section I, II, and III exhibit similar shapes with a single peak, but the maximum peak position and the peak range vary considerably. The maximum distribution coefficient is 1.06 $\times 10^{-22}$ m^2/s for section I, which is nearly one order of magnitude lower than those for sections II (1.47 $\times 10^{-21}$ m^2/s) and III (2.00 $\times$ 10^{-21} m^2/s). The peak for section I is larger and narrower compared to those for other two sections. Moreover, the total curve obtained for all regions is resolved as three peaks, which are corresponding to the diffusion coefficients of 3.50 $\times$ 10^{-25}, 9.26 $\times$ 10^{-22}, and 1.80 $\times$ 10^{-18} m^2/s. This result indicates that three different types of diffusivity exist in the N719/TiO_2 system, and that the adsorption process is essentially controlled by film diffusion.

Performance of dye-sensitized solar cells and kinetics of dye adsorption

The IPCE of DSSCs was analysed in term of the adsorption time of N719 (Fig. 3). The IPCE can be expressed as the product of three terms, as the following equation (7):[30,31]

$$\mathrm{IPCE} = \mathrm{LHE}(\lambda) \times \phi_{\mathrm{ini}} \times \eta_{\mathrm{coll}} \qquad (7)$$

where LHE is the light harvesting efficiency at a given wavelength (λ), Φ_{inj} is the quantum yield of charge injection, and η_{coll} is the efficiency of collecting the injected charge at the cathode.

Table 1. Adsorption kinetics model of N719 dye on a TiO_2 electrode

q_e, exp	Pseudo-first-order model			Pseudo-second-order model			Intra-particle diffusion model		
	q_e, cal (mmol/g)	k_1 (h^{-1})	$(R_1)^2$	q_e, cal (mmol/g)	k_2 (h·g/mmol)	$(R_2)^2$	k_{p1} ($h^{1/2}$·g/mmol)	k_{p2} ($h^{1/2}$·g/mmol)	k_{p3} ($h^{1/2}$·g/mmol)
0.087	0.072	0.297	0.943	0.081	20.092	0.999	0.029	0.004	0.001

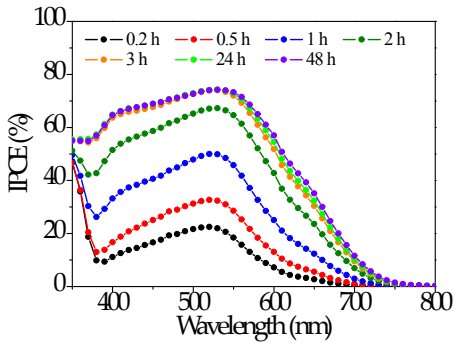

Fig. 3 Incident photon to current conversion efficiency spectra of DSSCs prepared using different dye adsorption times.

The LHE represents the fraction of incident photons absorbed by N719; and LHE can be expressed by equation (8):[31]

$$LHE = 1-10^{-abs(\lambda)} \quad (8)$$

where abs(λ) is the optical absorbance at wavelength λ of the N719 adsorbed on the TiO_2 film. Generally, the IPCE is expected to increase with the dye adsorption time. The IPCE may also increase with an increased amount of adsorbed dye, because the generated photocurrent is proportional to the amount of absorbed light in DSSCs. In this work, the FTO glass reflects ~20% of incident light. Therefore, about ~80% of the incident photons can be absorbed by the N719 and converted into photoelectrons.[31,32]

Fig. 3 shows the IPCE spectra of the DSSC as a function of the adsorption time. The IPCE increases as the adsorption time increases. The IPCE is especially enhanced in in the first 3 h of adsorption. The IPCE is saturated at about 75% efficiency for wavelengths ranging between 500 and 550 nm. In this region, there is a metal-to-ligand charge transfer (MLCT) transition, which causes the increased absorption. After 3 h, the dye coverage on the TiO_2 film approaches equilibrium, thus the IPCE is nearly saturated. The maxima of the IPCE spectra are shifted to longer wavelengths and are broadened compared to those for the earlier adsorption times.

Fig. 4a shows J_{sc} and η as a function of N719 adsorption time. The J_{sc} and η values are markedly enhanced in the time range of 0.2 - 3 h. The largest percentage of the dye molecules are adsorbed onto the TiO_2 electrode in this time range. Both the J_{sc} and η values are still increasing, but to a lesser extent, from 3-6 h, and are almost constant after 6 h. The number of adsorbed dye molecules does not increase after about 6 h. This trend is consistent with changes in the amount of adsorbed dye. Thus, we conclude that adsorption contact time plays a key role in increasing J_{sc} and η.[33]

Fig. 4b shows the change in the V_{oc} and *FF* as a function of adsorption time. The V_{oc} is 0.73 V, even early in the adsorption process, and then increases to a constant 0.75 V after sufficient dye adsorption. The small but increasing V_{oc} can be attributed to the decrease in electron-hole recombination from the conduction band of the TiO_2 film to I^{3-} in the electrolyte. In other words, the increasing density of the dye adsorption onto the TiO_2 electrode may insulate the TiO_2 surface from the electrolyte, which in turn hinders the electron transfer from the TiO_2 surface to the I^{3-} ions.[34]

The *FF* also increased sharply in the first 3 h, then decreases slightly from 3-6 h, and remains nearly constant at 68% after 6 hours. The coverage of the dye on the TiO_2 electrode increases and is chemisorbed to the interior surfaces of the micro-pores of the TiO_2, until the electrode is saturated. The morphology of the TiO_2 electrode and the charge recombination process are both contributing factors in the *FF* value of this DSSC.[35] Furthermore, the *FF* is also influenced by the dye adsorption times.

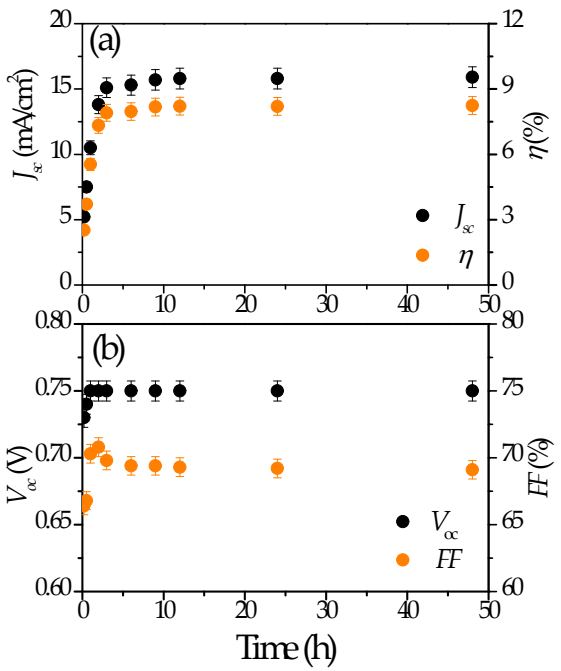

Fig. 4 The change in (a) J_{sc} and η, and (b) V_{oc}, and *FF* as a function of dye adsorption times.

Fig. 5a shows the transient absorption spectra of N719 on DSSC measured at different time intervals upon excitation with 540 nm. Transient absorption spectroscopy has proven particularly useful for investigating charge recombination and dye regeneration dynamics occurring in DSSCs.[36] The transient absorption band around 700-900 nm is attributed to the oxidized N719 species (cation radical, $N719^{+\bullet}$).[37] The transient absorption decay was observed at 824 nm, in which the contribution of the $N719^{+\bullet}$ is dominant.

Inset figure of Fig. 5b shows the transient absorption decay profile of DSSC for the dye-adsorption time of 48 h. A pseudo-second order exponential function was used to fit the decay kinetic profiles for long and short components. Here, the longer component is attributed to the back transfer of injected electrons from the TiO_2 conduction band to the $N719^{+\bullet}$, which corresponds to the charge recombination time (τ_{CR}). The shorter component can be assigned to the dye regeneration time (τ_{DR}) of $N719^{+\bullet}$ by I^- ions in the electrolyte (Fig. 6a).

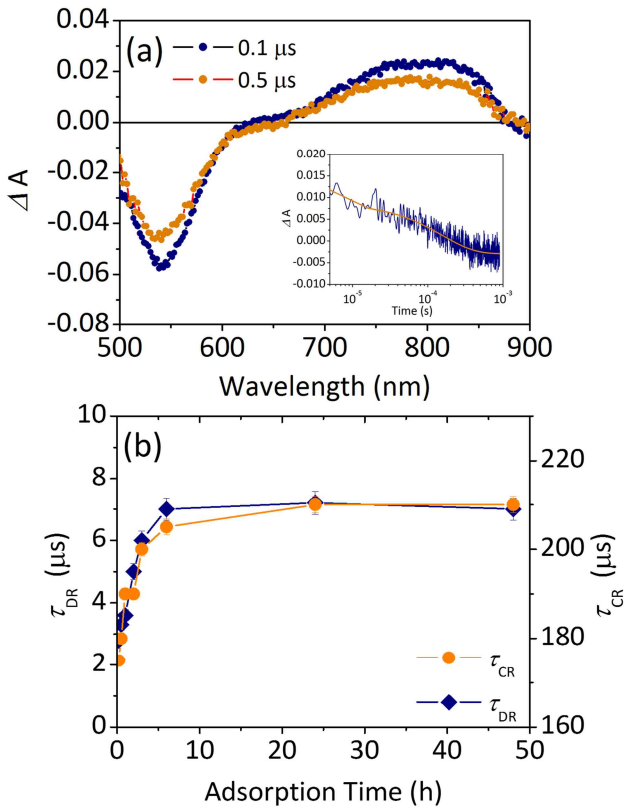

Fig. 6 (a) Transient absorption spectra and (b) charge-recombination (τ_{CR}) and dye-regeneration (τ_{DR}) time constants for DSSCs prepared with various dye adsorption times. The inset figure is the transient absorption decay profiles of DSSC prepared with dye-adsorption time of 48 h, and monitored at 824 nm.

The τ_{CR} and τ_{DR} were obtained from the transient absorption decay profiles of DSSCs prepared with different dye adsorption times as shown in Fig. 5b. Both τ_{CR} and τ_{DR} increased in conjunction with the increasing adsorption time as listed Table 2. Both τ_{CR} and τ_{DR} increased rapidly with the early dye adsorption time, and then became constant after about 6 h. These changes are similar with the changes of adsorption amount as shown in Fig. 2a.

Table 2. Charge-recombination (τ_{CR}) and dye-regeneration (τ_{DR}) time constants for DSSCs prepared with various dye adsorption times

adsorption time (h)	τ_{CR} (μs)	τ_{DR} (μs)	ϕ_{DR} (%)
0.2	175	2.8	98
0.5	180	3.3	98
1	190	3.6	98
2	190	5	97
3	200	6	97
6	205	7	97
24	210	7.2	97
48	210	7	97

*The monitoring wavelength was 824 nm.

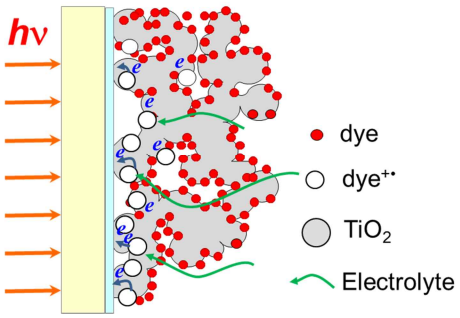

Fig. 6. Suggested mechanism for fundamental charge transport processes. It depicts that the photoelectrons and the oxidized dyes were generated at front of TiO_2 film.

The iodine ion concentration of the electrolyte plays a key role in dye regeneration dynamics (Fig. 6a).[38,39] The increasing of the τ_{DR} is directly attributed to the increasing diffusion resistance of I^- ion into the micro-pores of the TiO_2 electrode.[40] In general, rapid DR and slow CR processes are useful for obtaining high IPCE. In this work, the lifetimes of CR and DR processes increased with the same trend related to the increase of adsorption time (Fig 5b). This result indicates that the adsorption density of N719 on the TiO_2 electrode has an effect on the CR and DR characteristics of the DSSC system.

The light penetration depends on adsorbed dye concentrations, as described by Beer's law. The transmitted light-intensity decrease drastically according to the increase of the concentration of adsorbed dye. As shown in Fig. 6b, in case of highly dye-adsorbed DSSC, most of photoelectrons were generated predominantly from the front of DSSC, not from back. Therefore, the photoelectron can diffuse from front to back, and the CR process slows due to little chance to meet oxidized dye. Thus, the long CR time-constants are observed in DSSCs prepared with longer adsorption time. On the other hand, if the dye-oxidation takes place in front of TiO_2 film adsorbed dyes highly, the DR process become slower compared to that for short adsorption times. In order to reduce $N719^{+\bullet}$, the electrolyte should be diffused from back to front, because the surface diffusion of adsorbed $N719^{+\bullet}$ can be ignored. Therefore, both τ_{CR} and τ_{DR} increase with the increasing of dye adsorption times

The solar conversion efficiency is directly proportional to the dye-regeneration yield (ϕ_{DR}), which is defined as [41]

$$\phi_{DR} = \frac{k_{DR}}{k_{CR} + k_{DR}} \quad (9)$$

where k_{DR} is the rate constant of DR occurring in the presence of a redox couple (iodide/iodine), and k_{CR} is the rate constant of CR that takes place between the $N719^{+\bullet}$ and the injected electron in the conduction band of TiO_2. Based on the calculations using equation (9), the ϕ_{DR} values are determined to be >97% for all DSSC fabricated in this work as listed Table 2. This means that dye regeneration, and not charge recombination, is the main reduction process of $N719^{+\bullet}$.

Conclusions

In this study, we investigated the adsorption kinetics of N719 dye on the TiO_2 electrode of a DSSC using UV/Vis spectrophotometric measurements to monitor the adsorption processes directly. Several adsorption kinetics models were applied to explain the experimental kinetic data. Among many kinetic models tested in this work, the PSO model correlates well with the experimental adsorption data of the N719/TiO_2 electrode, indicating that chemisorption is the predominant adsorption process. Moreover, we also found from the diffusion-based model that film diffusion was the main controlling step of the system, even though the simultaneous occurrence of film and intra-particle diffusion was noticed. The models comparing the change in adsorption kinetics with dye adsorption time followed the variations in the main parameters (*FF*, V_{oc}, J_{sc}, and η) of DSSCs. In addition, the dye adsorption times (and dye adsorption amounts) influence the photodynamic processes such as DR and CR, which are also affected by the photoelectric properties of the DSSC.

Acknowledgements

This research was supported by Basic Science Research Program through the National Research Foundation of Korea (NRF) funded by the Ministry of Education (NRF-2013R1A6A3A03021144, K. -J. Hwang), (NRF-2014R1A1A-2004199, D. W. Cho).

Notes and references

1 B. O'Regan and M. Grätzel, *Nature*, 1991, **353**, 737.
2 A. Yella, H. W. Lee, H. N. Tsao, C. Yi, A. K. Chandiran, M. K. Nazeeruddin, E. W. Diau, C. Y. Yeh, S. M. Zakeeruddin and M. Grätzel, *Science*, 2011, **334**, 629.
3 (a) J. –H. Im, I. –H. Jang, N. Pellet, M. Grätzel and N. –G. Park, *Nature Nanotech*., 2014, 9, 927; (b) N. J. Jeon, J. H. Noh, Y. C. Kim, W. S. Yang, S. Ryu and S. I. Seok, *Nature Mat.*, 2014, **13**, 897; (c) W. S. Yang, J. H. Noh, N. J. Jeon, Y. C. Kim, S. Ryu, J. Seo, S. I. Seok, Science, 2015, DOI: 10.1126/science.aaa9272.
4 M. Grätzel, *J. Photochem. Photobiol. A: Chem.*, 2004, **164**, 3.
5 T. W. Hamann and J. W. Ondersma, *Energy Environ. Sci*., 2011, **4**, 370.
6 K. –J. Hwang, D. –W. Park, S. Jin, S. O. Kang and D. W. Cho, *Mater. Chem. Phys*., 2015, **149-150**, 594.
7 K.-J. Hwang, C. Im, D. W. Cho, S. -J. Yoo, J.-W. Lee and W. -G. Shim, *RSC Advances*, 2012, **2**, 3034.
8 K. –J. Hwang, J. –Y. Park, S. Jin, S. O. Kang and D. W. Cho, *New. J. Chem*., 2014, **38**, 6161.
9 (a) I. T. Choi, M. J. Ju, S. H. Song, S. G. Kim, D. W. Cho, C. Im, and H. K. Kim, *Chem. Eur. J*. 2013, **19**, 15545; (b) B. J. Song, H. M. Song, I. T. Choi, S. K. Kim, K. D. Seo, M. S. Kang, M. J. Lee, D. W. Cho, M. J. Ju, and H. K. Kim, *Chem. Eur. J*. 2011, **17**, 11115.
10 T. –Y. Kim, J. –W. Lee, E. –M. Jin, J. –Y. Park, J. –H. Kim, K. –H. Park, *Measurement*, 2013, **46**, 1692.
11 K. E. Noll, V. Gounaris and W. S. Hou, *Adsorption Technology for Air and Water Pollution Control*. Lewis Publishers INC., Michigan, 1992.
12 M. Suzuki, *Adsorption Engineering*. Kodansha & Elsevier, Tokyo & Amsterdam, 1990.
13 M. H. Kalavathy, T. Karthikeyan, S. Rajgopal, L. R. Miranda, *J. Colloid Interface Sci*., 2005, **292**, 354.
14 Q. Sun, L. Yang, *Water Res*., 2003, **37**, 1535.
15 J. Fan, W. Cai and J. Yu, *Chem. Asian J.*, 2011, **6**, 2481.
16 N. Kannan and M. M. Sundaram, *Dyes Pigments*, 2001, **51**, 25.
17 Y. S. Ho and G. McKay, *Proc. Biochem*., 1999, **34**, 451.
18 S. A. Azizian, *J. Colloid Interface Sci.*, 2006, **302**, 76.
19 A. L. Linsebigler, G. Lu and J. T. Yates, *Chem. Rev.*, 1995, **95**, 735.
20 J. R. Durrant, S. A. Haque and E. Palomares, *Chem. Rev.*, 2004, **248**, 1247.
21 C. Long, A. Li, H. Wu and Q. Zhang, *Colloid surf. A: Physicochem. Eng. Aspects*, 2009, **333**, 150.
22 H. Qiu, L. Lv, B. Pan, Q. Zhang and W. Zhang, *J. Zhejiang Univ. Sci. A*, 2009, **10**, 716.
23 H. K. Boparai, M. Joseph and D. M. O'Carroll, *J. Hazard. Materials,* 2011, **186***,* 458.
24 H. Chen and A. Wang, *J. Colloid Interface Sci.*, 2007, **307**, 309.
25 D. D. Maksin, S. O. Kljajević, M. B. Đolić, J. P. Marković, B. M. Ekmeščić, A. E. Onjia and A. B. Nastasović, *Hem. Ind.,* 2012, **66**, 795.
26 J. Crank, *The Mathematics of Diffusion*. Oxford University Press, London, England, 1956.
27 A. E. Ivanov, O. P. Kozynchenko, L. I. Mikhalovska, S. R. Tennison, H. Jungvid, V. M. Gun'ko and S. V. Mikhalovsky, *Phys. Chem. Chem. Phys.*, 2012, **14**, 16267.
28 K. V. Voitko, R. L. D. Whitby, V. M. Gun'ko, O. M. Bakalinska, M. T. Kartel, K. Laszlo, A. B. Cundy and S. V. Mikhalovsky, *J. Colloid Interface Sci.*, 2011, **361**, 129.
29 J. A. Nelder, R. Mead, *Computer Journal*, 1965, **7**, 308.
30 C. -R. Lee, H. –S. Kim, I. -H. Jang, J. -H. Im and N. -G. Park, *ACS Appl. Mater. Interfaces*, 2011, **3**, 1953.
31 A. Mihi, F. J. López-Alcaraz and H. Míguez, *Appl. Phys. Lett.*, 2006, **88**, 193110.
32 Y. Tachibana, H. Hara, K. Sayama and H. Arakawa, *Chem. Mater.*, 2002, **14**, 2527.
33 S. Sakaguchi, H. Ueki, T. Kato, T. Kado, R. Shiratuchi, W. Takashima, K. Kaneto and S. Hayase, *J. Photochem. Photobiol. A: Chem.,* 2004, **164**, 117.
34 S. A. Haque, Y. Tachibana, R. L. Willis, J. E. Moser, M. Grätzel, D. R. Klug and J. R. Durrant, *J. Phys. Chem. B*, 2000, **104**, 538.
35 T. W. Hamann, R. A. Jensen, A. B. F. Martinson, H. V. Ryswykac and J. T. Hupp, *Energy Environ. Sci.*, 2008, **1**, 66.
36 U. M. Tefashe, M. Rudolph, H. Miura, D. Schlettwein and G. Wittstock, *Phys. Chem. Chem. Phys.*, 2012, **14**, 7533.
37 J. E. Moser, D. Noukakis, U. Bach, Y. Tachibana, D. R. Klug, J. R. Durrant, R. Humphry-Baker and M. Grätzel, *J. Phys. Chem. B*, 1998, **102**, 3649.
38 D. Kuang, S. Ito, B. Wenger, C. Klein, J. –E. Moser, R. Humphry-Baker, S. M. Zakeeruddin and M. Grätzel, *J. Am. Chem. Soc.*, 2006, **128**, 4146.
39 J. N. Clifford, E. Martinez-Ferrero and E. Palomares, *J. Mater.* Chem., 2012, **22**, 12415.

40 X. Tang, Y. Wang and G. Cao, *J. Electroanal. Chem.*, 2013, **694**, 6.
41 K. –J. Hwang, D. W. Cho, J. –W. Lee and C. Im, *New. J. Chem*., 2012, **36**, 2094.